Results in Physics 8 (2018) 153–159

Contents lists available at ScienceDirect

Results in Physics

journal homepage: www.journals.elsevier.com/results-in-physics

Modeling and control for a magnetic levitation system based on SIMLAB platform in real time

Mundher H.A. Yaseen [a,*], Haider J. Abd [b]

[a] Gaziantep University, Electrical & Electronics Engineering Department, Gaziantep, Turkey
[b] Babylon University, College of Engineering, Department of Electrical Engineering, Iraq

ARTICLE INFO

Article history:
Received 19 October 2017
Received in revised form 21 November 2017
Accepted 21 November 2017
Available online 5 December 2017

Keywords:
Magnetic levitation system
Linear Quadratic Regulator (LQR)
PID control
Lead compensation

ABSTRACT

Magnetic Levitation system becomes a hot topic of study due to the minimum friction and low energy consumption which regards as very important issues. This paper proposed a new magnetic levitation system using real-time control simulink feature of (SIMLAB) microcontroller. The control system of the maglev transportation system is verified by simulations with experimental results, and its superiority is indicated in comparison with previous literature and conventional control strategies. In addition, the proposed system was implemented under effect of three controller types which are Linear–quadratic regulator (LQR), proportional–integral–derivative controller (PID) and Lead compensation. As well, the controller system performance was compared in term of three parameters Peak overshoot, Settling time and Rise time. The findings prove the agreement of simulation with experimental results obtained. Moreover, the LQR controller produced a great stability and homogeneous response than other controllers used. For experimental results, the LQR brought a 14.6%, 0.199 and 0.064 for peak overshoot, Setting time and Rise time respectively.

Introduction

Magnetic levitation technology is a perfect solution to achieve better performance for many motion systems, e.g., precision positioning, manipulation, suspension, and haptic interaction due to its non-contact, non-contamination, multi-Degrees-Of-Freedom (DOF), and long-stroke characteristics [1–4]. One of the features of maglev systems is reduction of imagination, which makes them enjoyable in the field of real-life applications [5], which are transportation systems [6], wind tunnel levitation [7], magnetic bearing systems and anti-vibration table [8]. These systems are inherently nonlinear and unstable as well. Therefore, the maglev system is also an interesting issue to confirm the performance of control schemes. However, many techniques were used to control these systems [9]. In [10] a real maglev system is controlled using PID. In [11], a feed forward multilayer neural network was used to model the system, in which learning and control is done simultaneously. As well as some works were done based on neural networks. Active neural networks for the pattern recognition are designed and implemented in [12]. Also, efficient techniques of adaptive controllers are investigated in [13,14]. In [15], stable neural controllers of nonlinear systems are designed. In [16], new iterative adaptive dynamic programming based optimum controllers are suggested and tested. Various methods for PI controller are design and have been tested [17–20].

However, the magnetic levitation system has unstable nonlinear dynamics which should be taken in count. Most of the contributions require measurements of position, velocity and electric current, and thus state observers should be synthesized to estimate the unavailable signals of the nonlinear dynamical system. Furthermore, it needs to design complex systems and some of these systems are costly. Considering the mention study, a controller to stabilize this system should be of great interest.

In this study, a model and a controller are introduced foran active method to control the maglev system based on SIMLAB platform. The maglev system used was verified experimentally and with simulations as well .The control systems were compared under various parameters. The findings showed an agreement for both simulation and experiment results.

Maglev system model

In this section, the construction of the magnetic levitation system and its components will be explained.

* Corresponding author.
E-mail addresses: mundheryaseen@gmail.com, my13436@mail2.gantep.edu.tr (M.H.A. Yaseen).

https://doi.org/10.1016/j.rinp.2017.11.026
2211-3797/

The proposed experimental magnetic levitation system is shown in Fig. 1. The system is made up 4 electromagnets as actuators for applying magnetic forces to achieve stable levitation and precise position control, a rigid square plate with 4 permanent magnets on each corner, and 4 Hall effect sensors for sensing the position of the levitating plate and Va is coil applied voltage.

The electromagnets are 15 mH solenoid coils with 2 Ω internal resistances. The Hall Effect sensors are linear radiometric Hall Effect sensors with 50 V/T. The permanent magnets are N52 neodymium disc magnets with 12.70 mm diameter and 6.35 mm thickness. The plate is a transparent acrylic plate with 152.4 mm × 152.4 mm × 3.175 mm. The frame is constructed by wood. For simplicity and tractability, the system is modeled using a quarter of the system (similar to a quarter car model). The model of the quarter-system is shown in Fig. 2, where R is the resistance of the coil, L is the inductance of the coil, v is the voltage across the electromagnet, i is the current through the electromagnet, m is the mass of the levitating magnet plus one-forth of the mass of the acrylic plate, g is the acceleration due to gravity, d is the vertical position of the levitating magnet measured from the bottom of the electromagnet, f is the force on the levitating magnet generated by the electromagnet and e is the voltage across the Hall effect sensor.

Case study

In this section, the mathematical model of maglev system has been presented.

The force actuated by the electromagnet is formulated as [21]

$$Fmag = C\frac{i(t)}{d^3} \tag{1}$$

where (t) denotes the current across the electromagnet, d is the vertical position and C is a constant related to turn ratio and cross sectional area of the electromagnet.

From a force balancing equation, we have

$$M\ddot{d} = mg - C\frac{i(t)}{d^3} \tag{2}$$

where m is the mass of the levitating magnet plus one-fourth of the mass of the acrylic plate and g is the is the acceleration due to gravity,

In addition, an electrical relation of the voltage supply and the electromagnetic coil can be expressed by

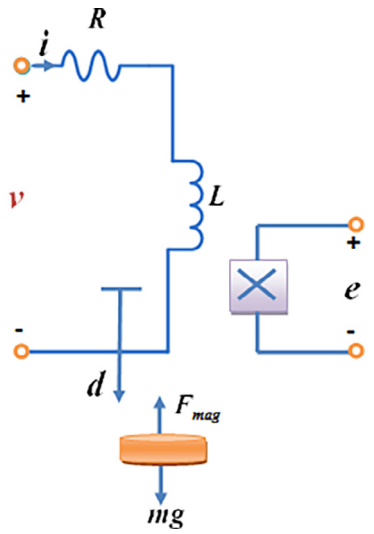

Fig. 2. Electromagnetic levitation system model.

Table 1
Proposed system parameter.

	Parameter	Value	Unit
Sensor	β	5.64×10^{-4}	$V.m^2$
	γ	0.31	V/A
	α	2.48	V
Operation point	i_0	1	A
	d_0	20	mm
Electromagnet	C	2.4×10^{-6}	Kgm^5/s^2A
	R	2	Ω
	L	15×10^{-3}	H
	m = M/4	0.02985	kg

$$v(t) = R.i(t) + L\frac{di}{dt} \tag{3}$$

where R and L are resistance and inductance of the electromagnet respectively. Now consider the following perturbations with respect to the change of them

$$i(t) = i_0 + \Delta i(t)$$

$$d(t) = d_0 + \Delta d(t) \tag{4}$$

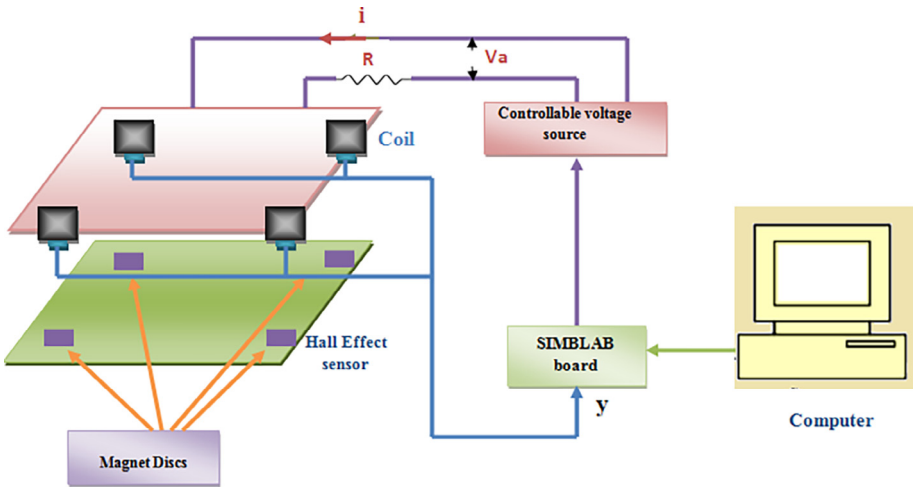

Fig. 1. Free body diagram of magnetic levitation system.

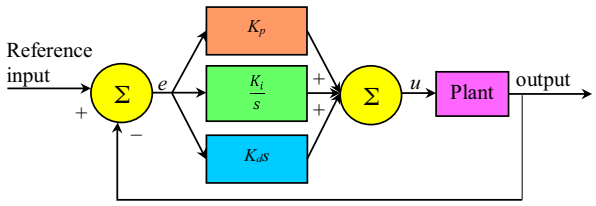

Fig. 3. Block diagram of PID controller.

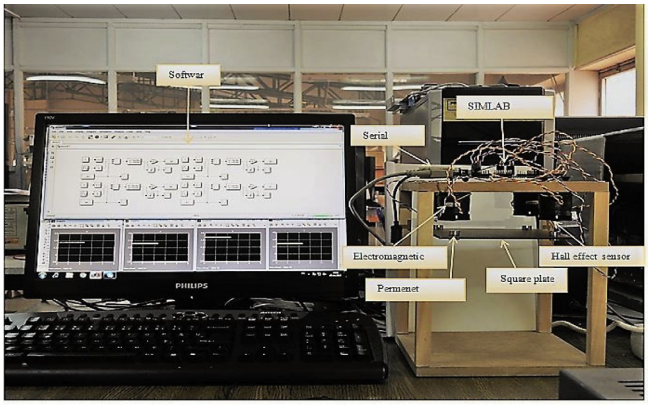

Fig. 4. Experimental setup of magnetic levitation system.

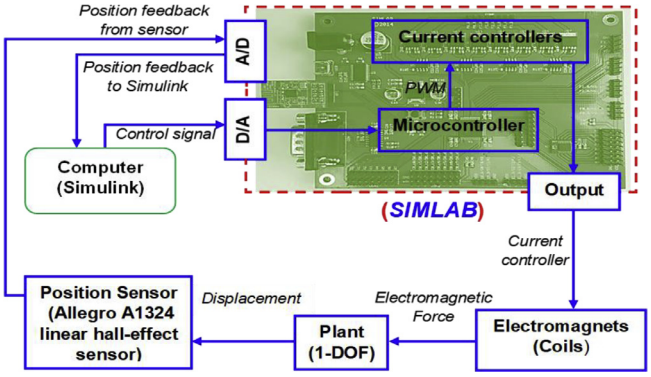

Fig. 5. Interfacing of maglev system with SIMLAB Platform.

$$v(t) = v_0 + \Delta v(t)$$

where v_o is the required equilibrium coil voltage to suspend the levitating plate at d_o

Under this perturbation, the dynamics (2) and (3) around an operating point (i_0, d_0, v_0) can be linearized as

$$m\ddot{\Delta d} = \left(\frac{3Ci_0}{d_0^4}\right)\Delta d - \left(\frac{C}{d_0^3}\right)\Delta i \tag{5}$$

$$\dot{\Delta i} = -\frac{R}{L}\Delta i - \frac{1}{L}\Delta v \tag{6}$$

where Δi, Δv, Δd is linearization of the system about the equilibrium point.

After eliminating Δi in (6) and applying Laplace transforms, we obtain the transfer function from Δv to Δd given as

$$\frac{\Delta D(s)}{\Delta V(s)} = \frac{-\frac{gR}{v_0}}{(Ls+R)\left(s^2 - \frac{3Ci_0}{md_0^4}\right)} \tag{7}$$

where $\Delta V(s)$ and $\Delta D(s)$ denote the Laplace transforms of $\Delta v(t)$ and $\Delta d(t)$, respectively.

Hall sensor has an output voltage of the given form [22]

$$e(t) = \alpha + \frac{\beta}{d^2} + \gamma i(t) \tag{8}$$

where α, β, γ are constant sensor parameters. A linearization of (8) around $e(t) = e_0 + \Delta e$ results in

$$\Delta e = -\frac{2\beta}{d_0^3}\Delta d + \gamma \Delta i \tag{9}$$

where Δe is the sensor voltage

Applying Laplace transform to (9) and using $I(s) = \Delta V(s)/(Ls + R)$ from (3) and the representation in (7), we obtain a relation between the electromagnet voltage $\Delta V(s)$ and a sensor voltage perturbation $\Delta E(s)$ as follows;

$$\frac{\Delta E(s)}{\Delta V(s)} = \frac{\gamma\left(s^2 - \frac{3Ci_0}{md_0^4}\right) + \frac{2\beta RC}{md_0^6}}{(Ls+R)\left(s^2 - \frac{3Ci_0}{md_0^4}\right)} \tag{10}$$

Eq. (10) can represent also in the state space form after applying the second derivative of (5) and first derivative of (6). Thus, the state space representation of the linearized model of Eq. (10) can be represented by followings:

$$\begin{bmatrix}\dot{x}_1\\ \dot{x}_2\\ \dot{x}_3\end{bmatrix} = \begin{bmatrix}0 & 1 & 0\\ 3\frac{C}{m}\frac{i_0}{d_0^4} & 0 & -\frac{C}{m}\frac{1}{d_0^3}\\ 0 & 0 & -\frac{R}{L}\end{bmatrix}\begin{bmatrix}x_1\\ x_2\\ x_3\end{bmatrix} + \begin{bmatrix}0\\ 0\\ \frac{1}{L}\end{bmatrix}u \tag{11}$$

The measured output system (y) can be obtained after simplified Eq. (9),where ($\Delta e = y$, $\Delta d = x_1$, and $\Delta i = x_3$)

$$y = \begin{bmatrix}-2\frac{\beta}{d^3} & 0 & \gamma\end{bmatrix}\begin{bmatrix}x_1\\ x_2\\ x_3\end{bmatrix} \tag{12}$$

Suppose that $x = [x_1\ x_2\ x_3] = [d\ \dot{d}\ i]$ is the state of the system, where d is the controlled output, $y = e$ is the measured output and $u = v$ is the control input

By substituting system parameters in Table 1 into (10),

$$G(s)H(s) = \frac{20.66s^2 + 61803}{s^3 + 132.5s^2 - 1471s - 194900} \tag{13}$$

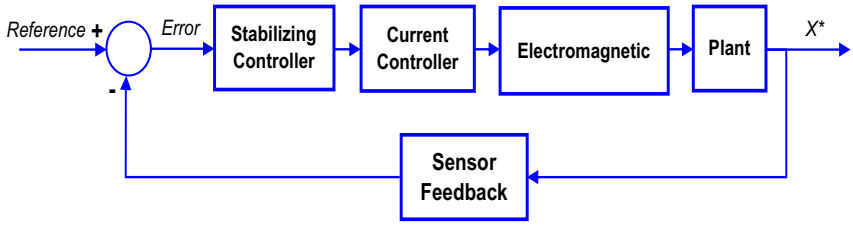

Fig. 6. Closed loop block diagram of Maglev system.

The numerical values of the state space equations are given below

$$\begin{bmatrix}\dot{x}_1\\ \dot{x}_2\\ \dot{x}_3\end{bmatrix}=\begin{bmatrix}0 & 1 & 0\\ 1471 & 0 & -9.81\\ 0 & 0 & -133\end{bmatrix}\begin{bmatrix}x_1\\ x_2\\ x_3\end{bmatrix}+\begin{bmatrix}0\\ 0\\ 66.66\end{bmatrix}u \tag{14}$$

$$y=\begin{bmatrix}-144 & 0 & 0.31\end{bmatrix}\begin{bmatrix}x_1\\ x_2\\ x_3\end{bmatrix} \tag{15}$$

Controller system design

This section deals with the development of LQR based controller, PID control and Lead Compensation for magnetic levitation system as follows:

Linear Quadratic Regulator (LQR) controller

The Linear Quadratic Regulator (LQR) method is similar to Root Locus approach by inserting the closed loop poles of the system into the desired location [16]. The EMS linearization dynamic model is formulated by state space as in below:

$$\dot{x}(t)=Ax(t)+Bu(t) \tag{16}$$

$$y(t)=Cx(t)+Du(t) \tag{17}$$

The $x(t)$ state can be measured and the cost function of constructing controller can be minimized based on the formula below:

$$J(u)=\int_0^{+\infty}(x^T(t)Qx(t)+u^T(t)Ru(t))dt \tag{18}$$

where Q and R values that can be considered positive definite weighting matrices. For initial state condition, the variable $x(0)$ Considered as a steady state based on perturbation of the control system. The first term of the $J(u)$ Function considered as cost subject which is assigned to the energy in transient response.

The control signal $u(t)$ is considered as linearly proportional to the specified air gap. Also, its proportional to the clearance of track boundary condition at desired operating point (i_o, z_o) in design stage.

Used by the linear state feedback can be expressed by the equation below:

$$u(t)=-[k_p(x_1(t)-z_{ref})+k_v(x_2(t))+k_a(x_3(t))] \tag{19}$$

where: k_p represents the steady error, k_v control suspension damping and k_a taken for all stability margins. The linear controller limitations considered as the ability to suppress disturbances in the control loop. The LQR gains calculated are [k_p = 32,483, k_v = 90.4, k_a = −9.4] .

PID controller

The schematic diagram of PID controller is given in Fig. 3. This control system is working based on the calculations of the error value, trying to reduce the error percentage by adjusting the controller parameters. The general form of this controller formulated as in below [18]:

$$u(t)=K_p\left(e(t)+\frac{1}{T_i}\int_0^t e(\tau)d\tau+T_d\frac{de(t)}{dt}\right) \tag{20}$$

where:

$u(t)$: denote the control signal Kp: the proportional gain, Ti: integral time Td: derivative time, Kp, Ti, Td: the control parameters for tuning and

$e(t)$: the difference between the reference point and actual plant.

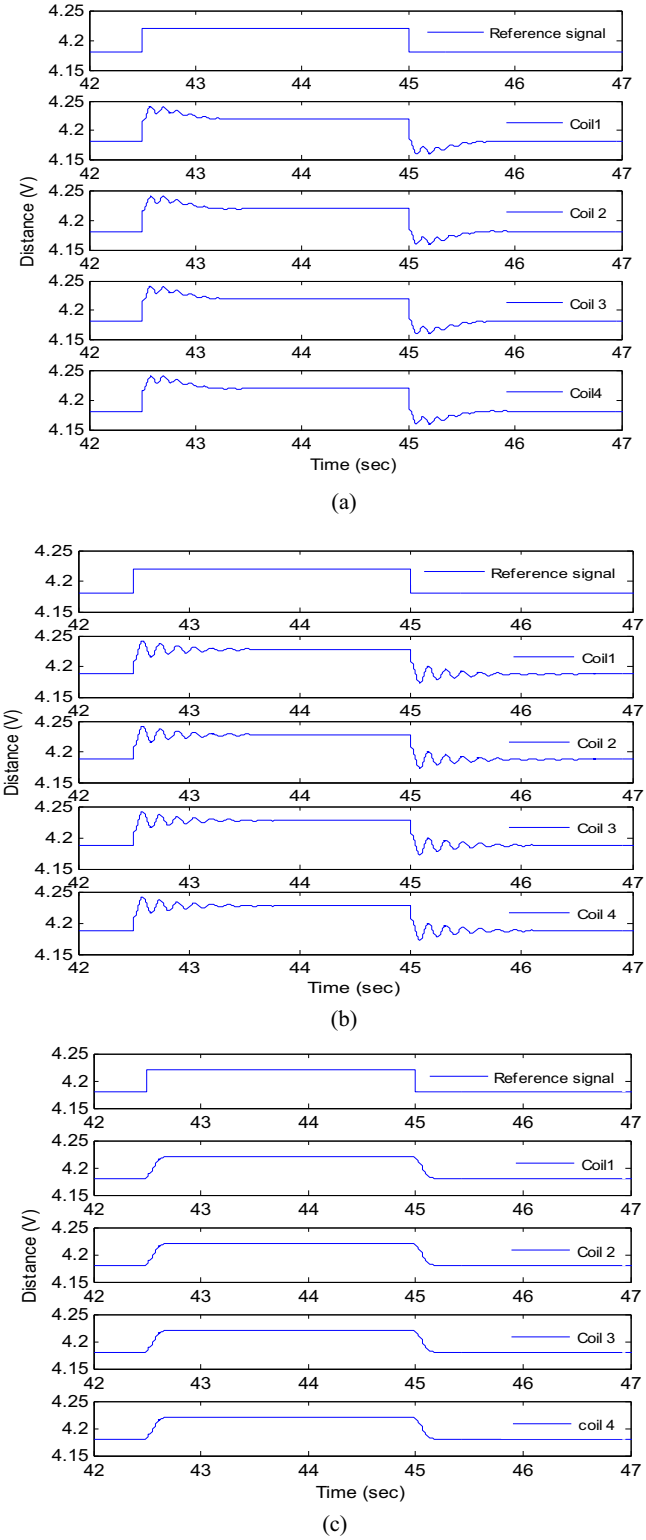

Fig. 7. Simulation results of magnetic levitation system for a square wave input signal using (a) PID, (b) Lead and (c) LQR controllers.

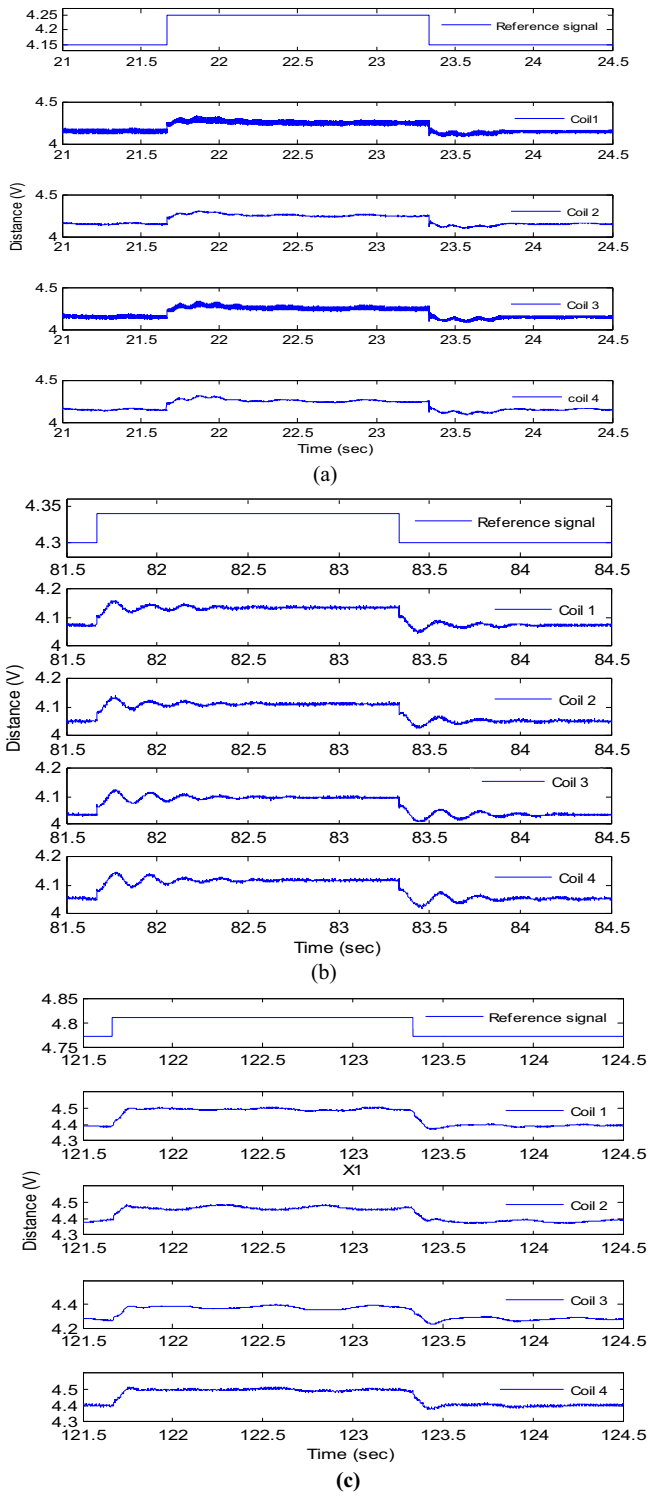

Fig. 8. Real-time results of magnetic levitation system for a square wave input signal using (a) PID, (b) Lead and (c) LQR controllers.

By placing the closed loop poles at P = [−132.45 38.36–28.36], the PID gains calculated are [Kp = 10, K_I = 4, K_D = 0.2].

Lead compensation

Lead compensation controller design controller is one of the mainly methods which is used in industrial applications. Phase lead compensation control can be classified as a classical control category. It is almost used feedback controller, for that it's widely applied in industrial control systems [22]. Mitigating error percentage is the working principle of the lead compensation controller by adjusting the control system parameters. Eq. (21) explains the structure of the phase lead compensator with adding the zero and pole to the transfer function. The transfer function can be written as follows:

$$G_c(S) = K_c.\alpha\frac{Ts+1}{\alpha Ts+1} = K_c\frac{s+\frac{1}{T}}{s+\frac{1}{\alpha T}} = K_c\frac{s+Z}{s+P} \quad (21)$$

where: $G_c(s)$: transfer function, (K_cT_s): the control parameters where, K_c is compensator in close loop system, Z is zero and P is pole. By integrating the transfer function of the lead compensator via the Matlab, it can obtain the optimized transfer function (update parameters) which is applied on the proposed magnetic levitation system and figured the system output. The lead compensating parameters calculated are [K_c = 10, Z = 30, P = 100].

Table 2
Comparison between Simulation results and Experimental results of magnetic levitation system.

Controller	Rise time (s)	Peak overshoot%Mp	Settling time (s)
Simulation Results			
PID	0.013	43.6	0.623
Lead	0.040	39.3	0.196
LQR	0.115	0.505	0.102
Experimental Results			
PID	0.017	54.4	1.42
Lead	0.042	41	0.2
LQR	0.064	14.6	0.199

Results and discussion

In this section, the experimental and simulation results were obtained based on different parameters and according to the proposed system design in Fig. 4.

In this paper, three types of controllers were applied to the electromagnetic levitation prototype. The interfacing of hardware controlled unit parts are explained in Fig. 5. A real-time control feature of simulink which supports the microcontroller (SIMLAB) has been employed. Feedback control for this system is designed utilizing linear control theory. The overall architecture comprising of data acquisition hardware (SIMLAB) sensor, electromagnetic coils and real-time operating environment is shown in Fig. 5. The (SIMLAB) platform is a versatile, complete and low-cost real-time package with 15.2 kHz sampling rates. Moreover, (SIMLAB) is fully integrated into MATLAB and simulink with highly intuitive usage. A conversion of displacement sensor signal to digitized value is first carried out using analog to digital (A/D) converter. The stability controller processed digitized value and send it through computer to digital to analog (D/A) port of the microcontroller. Microcontroller produces control current corresponding to coil magnetic field. The generated PWM value is then sent to current controller to produce corrective control current i.e., electromagnetic force. Therefore, since the load is varied and position has to be maintained, then feedback control will adjust the strength of the magnetic field to hold the suspended object in the desired position. The block diagram representation of overall control system is illustrated in Fig. 6, where the X^* is the desired output.

The simulation results of the system are shown in Fig. 7. From the simulation results indicating in Fig. 7, after applying the square wave input signal on the system and in the available of LQR controller the system performance was stable and its responds are perfect compared to PID and Lead compensation which offers less stability and slower response. Where the output signals figured at

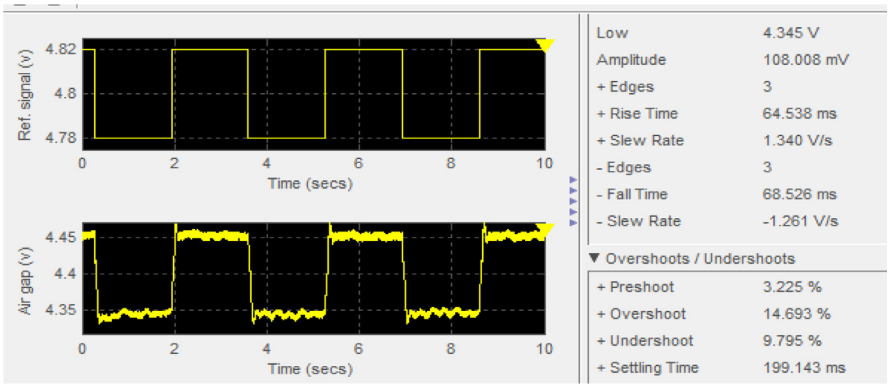

(a)

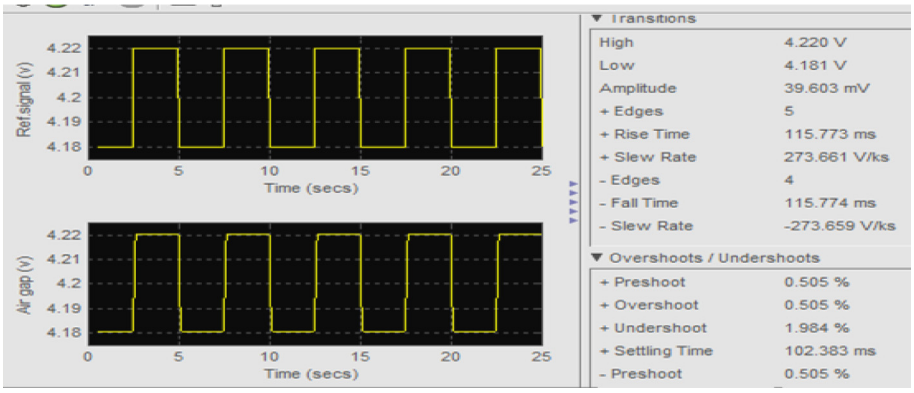

(b)

Fig. 9. Time waveform using LQR controllers of (a) Real time, and (b) simulation.

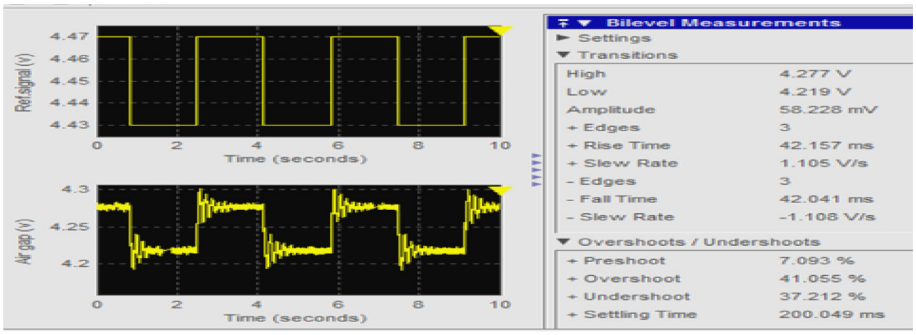

(a)

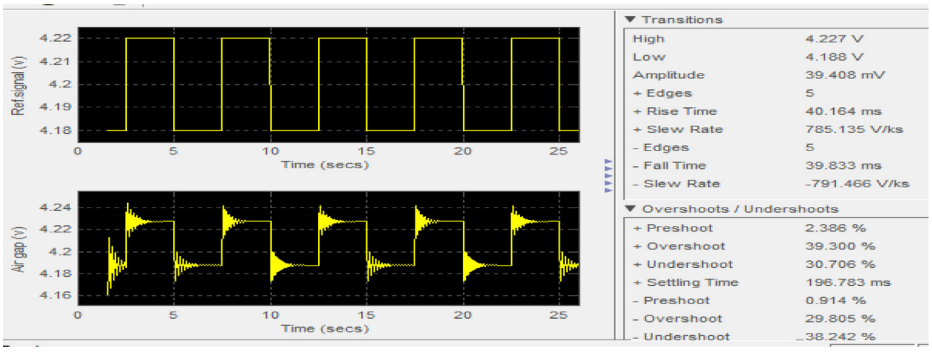

(b)

Fig. 10. Time waveform using Lead controllers of (a) Real- time, and (b) simulation.

the four coils are almost identical to the reference input signal. Furthermore The controller exhibit more robustness in performance compared with the used controllers, represented by minimum peak overshoot in the range of 0.505%, and an optimum values of setting time and Rise time of 0.102 and 0.115 respectively, which is better than PID and Lead controller, as in Table 2. Subsequent as in Fig. 8, the experimental results verified the simulation results. System outputs display the same behavior and trend in the system response criteria when the system was implemented with the simulation. The real-time results explained that LQR controller introduced efficient response and better stability than PID and Lead compensation under the effect of same input signal and parameters. The little difference in the results between simulation and experiment that some parameter assumption has been neglected in the simulation. Figs. 9 and 10 shows the time waveform results for both LQR and Lead controller. Table 2 shows the all simulation and experimental results for all controllers utilized.

Conclusion

This paper investigates the modeling and design of a real-time magnetic-levitation (maglev) system. The control scheme for the maglev transportation system has been implemented experimentally and it was verified by the simulations. Furthermore, the suggested system was performing with three types of controller which are LQR, PID and Lead compensation. The controller's types have been compared in term of three parameters which are peak overshoot, Rise time and settling time. The findings displayed an agreement of experimental with simulation results were obtained. Moreover, the LQR controller showed higher stability and response in comparison with classical controller types used for all the system parameters utilized. Experimentally, the LQR appeared a 14.6%, 0.199 and 0.0.64 for Peak overshoot, Setting time and Rise time respectively.

References

[1] Ono M, Koga S, Ohtsuki H. Japan's superconducting Maglev train. IEEE Instrum Meas Mag 2002;5(1):9–15.

[2] Chen Mei-Yung, Wang Ming-Jyh, Li-Chen Fu. A novel dual-axis repulsive maglev guiding system with permanent magnet: modeling and controller design. IEEE/ASME Trans Mechatron 2003;8(1):77–86.

[3] de Boeij Jeroen, Steinbuch M, Gutierrez H. Real-time control of the 3-DOFsleddynamics of a null-flux Maglev system with a passive sled. IEEE Trans Magn 2006;42(5):1604–10.

[4] Rote D, Cai Yigang. Review of dynamic stability of repulsive-force maglev suspension systems. IEEE Trans Magn 2002;38(2):1383–90.

[5] Cho D, Kato Y, Spilman D. Sliding mode and classical control of magnetic levitation systems. IEEE Control Syst Mag 1993;13(1):42–8.

[6] Jayawant BV, Sinha PK, Aylwin DG. Feedback Control System for D.C. Electromagnets in Passenger-Carrying Vehicles. Int J Control 1976;24 (5):627–39.

[7] Covert EE, Vlajinac M, Stephens T, Finston M, Magnetic Balance and Suspension System for use with Wind Tunnels, In: Kuchemann D, editor. Progress in Aerospace Science, vol. 14, Pergamon Press; 1973. pp. 27–107.

[8] Kosuke N, Masashi I. A noncontact permanent magnet levitation table with electromagnetic control and it's vibration isolation method using direct disturbance cancellation combining optimal regulators. IEEE Tran On Magnetics Jan 1995;31(1).

[9] Huang Chao-Ming, Yen Jia-Yush, Chen Min-Shin. Adaptive nonlinear control of repulsive maglev suspention system. Control Eng Pract 2000.

[10] Zomorodian A, Menhaj MB, Daghooghi Z, Saboori I, A Real Time Digital Controller for Magnetic Levitation System, Second IEEE.

[11] Soloway Donald, Haley Pamel J. Neural generalized predictivecontrol: a newton-raphson implementation. NASA Technical Memorandum Feb 1997;110244.

[12] Hartert L, Sayed-Mouchaweh M. Dynamic supervised classification method for online monitoring in non-stationary environments. Neurocomputing 2014;126:118–31.

[13] Iglesias JA, Skrjanc I. Applications, results and future direction. Evol Syst 2014;5:1–2.

[14] Lughofer E, Sayed-Mouchaweh M. Adaptive and on-line learning in non-stationaryenvironments. Evol Syst 2015;6:75–7.

[15] Meda-Campaña JA, Rodriguez-Valdez J, Hernandez-Cortes T, Tapia-Herrera R, Nosov V. Analysis of the fuzzy controllability property and stabilization for a class of T-S fuzzy models. IEEE Trans Fuzzy Syst 2015;23(2):291–301.

[16] Sayed-Mouchaweh M, Lughofer E. Decentralized fault diagnosis approach without a global model for fault diagnosis of discrete event systems. Int J Control 2015;88(11):2228–41.

[17] Iterative auto-calibration of digital controllers. Methodology and applications. Control Eng Pract 1998;6(3):345–58.

[18] PI and PID controllers tuning for integral-type servo systems to ensure robust stability and controller robustness, Electrical Engineering, vol. 88, no. 2, pp. 149–156, 2006.

[19] Robust gain scheduled control of a hydrokinetic turbine, IEEE Transactions on Control Systems Technology, vol. 19, no. 4, pp. 805–817, 2011.

[20] IMC-PID design based on model matching approach and closed-loop shaping, ISA Transactions, vol. 53, no. 2, pp. 462–473, 2014.

[21] Cheng DK. Field and Wave Electromagnetics. MA: Addison-Wesley; 1983.

[22] Smaili A, Mrad F. Applied Mechatronics. MA: Oxford; 2008.